arXiv:cond-mat/0412400v1 [cond-mat.soft] 15 Dec 2004

Elastic medium confined in a column versus the Janssen experiment.

G. Ovarlez[1,2*], E. Clément[2]
[1] *Laboratoire des Matériaux et Structures du Génie Civil - UMR 113 (LCPC-ENPC-CNRS) Institut Navier - 2, allée Kepler - 77420 Champs sur Marne - France*
[2] *Physique et Mécanique des Milieux Hétérogènes (UMR 7636 CNRS-ESPCI) and Université Pierre et Marie Curie ESPCI - 10, rue Vauquelin - 75231, Paris Cedex 5 - France*

(Dated: March 23, 2022)

We compute the stresses in an elastic medium confined in a vertical column, when the material is at the Coulomb threshold everywhere at the walls. Simulations are performed in 2 dimensions using a spring lattice, and in 3 dimensions, using Finite Element Method. The results are compared to the Janssen model and to experimental results for a granular material. The necessity to consider elastic anisotropy to render qualitatively the experimental findings is discussed.

PACS numbers:

I. INTRODUCTION

The mechanical status of granular matter is presently one of the most open and debated issues [1]. This state of matter exhibits many unusual mechanical and rheological properties such as stress induced organization at the microscopic [2] or at the mesoscopic [3] level which may yield macroscopic effects such as stress induced anisotropy [4, 5]. This issue sets fundamental questions relevant to the understanding of many other systems exhibiting jamming such as dense colloids or more generally soft glassy materials [6, 7]. For practical applications, the quasistatic rheology of granular assemblies is described using a phenomenological approach, based on an elasto-plastic modelling of stress-strain relations [8]. So far, there is no consensus on how to express correctly the macroscopic constitutive relations solely out of microscopic considerations and under various boundary conditions or loading histories. This very basic issue was illustrated in a recent debate on how to understand the stress distribution below a sand pile and especially how to account for the dependence on preparation protocols [9]. A new mechanical approach was proposed based on the concept of "fragile matter" [7] and force chains propagation modelling [10]. But recent experiments have dismissed this approach and evidenced results more consistent with the traditional framework of general elasticity [11].

In this paper we focus on the predictions for stresses measurements at the bottom for an elastic material confined in a rigid cylinder. When the column is filled with granular material it corresponds to the classical Janssen's problem [12]. Recently, this issue has received a lot of attention either experimentally [13, 14, 15, 16, 17, 18, 19] or numerically [20, 21], the confined material being either pushed or pulled down. Surprisingly, so far to our knowledge, there are very few systematic comparison or even direct relation with the outcome of standard elasticity in the same situation of confinement. Note that experimentally, it was found that essentially elastic materials like gels, may display a Janssen stress saturation effects that could well predict the onset of self-collapsing under gravity [22]. In a recent paper [23], Evesque and de Gennes proposed a model for the slow filling of an elastic medium modelling a granular packing. As the material is poured in the column, displacements of the material at the bottom are induced by the weight of the new material added so that it mobilizes friction forces. Within the assumption of a minimal anchorage length, it leads to partial and inhomogeneous mobilization of friction at the walls: friction is fully mobilized at the bottom, and partially in the upper part of the column. A Janssen like pressure profile can be derived in the case where the saturation length λ is high compared to the column radius R; this last condition is actually restrictive and inappropriate for usual experimental cases [13, 16].

We propose to study in detail the elastic predictions and to compare them to the Janssen model and to experimental results for a granular material in *the same situation* i.e. when the material is at the Coulomb threshold *everywhere* at the walls. The main comparison features with the experimental results have already been presented in [16]; here, we detail much more the elastic predictions.

Two kinds of situations are considered. First, the mass at the bottom of the column is measured as a function of the material filling mass. Second, similar measurements are produced with an overweight on the top of the material. We recently performed the corresponding experiments for a granular material [16] and it was shown that one could obtain quite reproducible data provided a good control of the packing fraction homogeneity and a polarization of all the friction forces at the walls in the upwards direction. Our measurements confirmed, for the first time, the general

* author to whom correspondence should be addressed: ovarlez@lcpc.fr

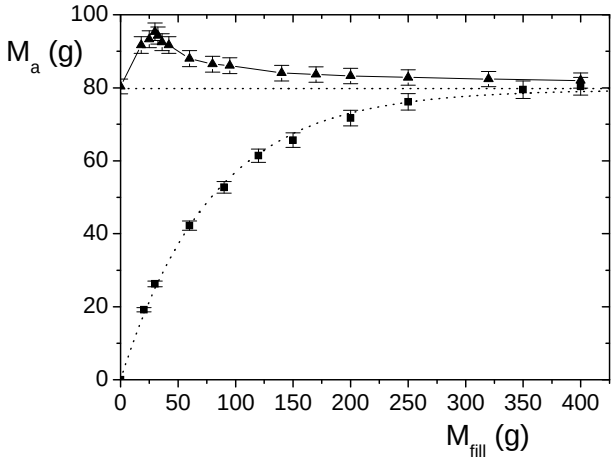


FIG. 1: Apparent mass M_a vs. filling mass M_{fill} for a loose packing ($\bar{\nu} = 59\%$) of slightly polydisperse 1.5 mm glass beads in a 38 mm diameter steel column of friction coefficient $\mu_s = 0.25$ without an overweight (squares), and with a 80.5 g overweight (triangles, line) on top of the granular material. The results of both experiments are compared to the Janssen model prediction (dotted lines).

validity of Janssen's saturation curve. They also evidenced an overshoot effect of spectacular amplitude induced by a top mass equal to the saturation mass. These experimental results are actually strong tests for any theory of granular matter.

II. EXPERIMENTAL RESULTS AND JANSSEN MODEL

We first summarize our recent experimental results [16] and compare them to the Janssen model predictions. In [16], a slightly polydisperse assembly of 1.5 mm glass beads was poured at controlled packing fraction in steel columns of various friction coefficient, and of diameter varying between 38 mm and 80 mm. The aim of the experimental procedure is to achieve the Coulomb threshold everywhere at the walls when the apparent mass M_a is measured; see [16] for details on the procedure. The apparent mass M_a measured at the bottom of the column was plotted as a function of the filling mass M_{fill} of the material. The typical results obtained when M_{fill} is varied are shown on Fig. 1. The apparent mass M_a saturates exponentially with M_{fill}. When an overweight equal to the saturation mass M_{sat} is added on top of the granular material, M_a increases with M_{fill}, up to a maximum M_{max}, which is about 20% higher than M_{sat}, then decreases slowly towards the saturation mass M_{sat}.

The simple model which captures the physics of this saturation phenomenon was provided in 1895 by Janssen [12]. This model is based on the equilibrium of a granular slice taken at the onset of sliding everywhere at the walls; we attempted to realize as best as possible this last condition in our experiment [16]. In cylindrical coordinates with origin at the top surface and the cylinder axis being the z axis, the relation, at the slipping onset, between the shear stress σ_{rz} and the horizontal stress σ_{rr} at the walls is

$$\sigma_{rz}(r{=}R, z) = \mu_s \sigma_{rr}(r{=}R, z) \tag{1}$$

where μ_s is the Coulomb static friction coefficient between the grains and the walls. It results in a relation between the filling mass M_{fill} and the apparent mass at the bottom M_a of the form:

$$M_a = M_{sat}(1 - \exp(-\frac{M_{fill}}{M_{sat}})) \tag{2}$$

with

$$M_{sat} = \frac{\rho \pi R^3}{2K\mu_s} \tag{3}$$

where ρ is the mass density of the granular material, and K is the Janssen parameter rendering the average horizontal redirection of vertical stresses:

$$\sigma_{rr} = K\sigma_{zz} \tag{4}$$

From a mechanical point of view, a major simplification of this model comes from the assumption that the redirection parameter K would stay constant along the vertical direction. But on the other hand, it provides a clear and simple physical explanation for the existence of an effective screening length $\lambda = R/2K\mu_s$ above which the mass weighted at the bottom saturates.

In [16], several saturation profiles were measured for various packing fractions, columns sizes and friction coefficients between the grains and the walls. When the apparent mass rescaled by the saturation mass is plotted as a function of the filling mass also rescaled by the saturation mass, we obtain a *universal rescaling* of all data on a curve which is precisely the one predicted by Janssen (Fig. 1): $M_a/M_{sat} = f(M_{fill}/M_{sat})$, with $f(x) = 1 - \exp(-x)$. The rescaling with radius R and friction coefficient μ_s was also checked, and good agreement with the Janssen model rescaling was found. The Janssen constant K was found to depend on packing fraction $\bar{\nu}$ and an effective relation was derived: $\Delta K/K \simeq 5\Delta\bar{\nu}/\bar{\nu}$. On the other hand, when a top mass equal to the saturation mass is added on the top of the granular material, the apparent mass M_a displays a maximum M_{max} 20% higher than M_{sat}, whereas the Janssen model predicts $M_a = M_{sat}$ whatever the filling mass M_{fill} is. Therefore, this overshoot goes beyond the possibilities of Janssen's model which seems adapted to a unique configuration.

In the next section, we study in detail the predictions of isotropic homogeneous elasticity.

III. ELASTICITY: THEORY AND SIMULATION METHODS

A. Theory

We first recall the general framework of homogeneous isotropic elasticity, and then predict the behavior of an elastic material confined in a column.

The elastic theory gives, in the limit of small deformations, a linear relation between the stress tensor components σ_{ij} and the strain tensor components ϵ_{ij}. For an isotropic elastic material, we get

$$E\epsilon_{ij} = (1+\nu_p)\sigma_{ij} - \nu_p\delta_{ij}\sigma_{kk} \tag{5}$$

where E is the Young modulus, and ν_p the Poisson ratio which takes its value between -1 and $1/2$ in 3D, and between -1 and 1 in 2D.

In a uniaxial homogeneous compression experiment (Fig. 2), where $\sigma_{zz} = -p$ is imposed everywhere, the other stress tensor components being null, we get

$$\epsilon_{zz} = -p/E \tag{6}$$

everywhere and

$$\epsilon_{xx} = \epsilon_{yy} = -\nu_p\epsilon_{zz} \tag{7}$$

which signifies that the material expands in the transverse direction.
The Young modulus E is thus characteristic of the material's stiffness; a cylinder of length l and section S has stiffness $k = ES/l$ in the axial direction. The Poisson ratio is linked to the material compressibility: the volume variation is: $\delta V/V = -(1-2\nu_p)p/E$. Therefore, an incompressible material has Poisson ratio $1/2$ in 3D (1 in 2D).

If we now confine an elastic medium of Young modulus E and Poisson ratio ν_p, in a rigid cylinder of radius R, no more radial displacement at the walls is allowed: $u_r(r=R) = 0$. Stresses and displacements can actually be calculated in the *limit of high depths* z under the assumption that they then should be independent of z. The boundary conditions we impose are the Coulomb condition everywhere at the walls

$$\sigma_{rz}(r{=}R) = \mu_s\sigma_{rr}(r{=}R) \tag{8}$$

and infinitely rigid walls i.e. $u_r(r{=}R) = 0$. The stress tensor components are then

$$\sigma_{rz}(r,z) = -\frac{1}{2}\rho g r \tag{9}$$

$$\sigma_{rr} = \sigma_{\theta\theta} = \frac{\nu_p}{1-\nu_p}\,\sigma_{zz} \tag{10}$$

$$\sigma_{zz}^{sat}(r,z) = -\frac{(1-\nu_p)\rho g R}{2\nu_p\mu_s} \tag{11}$$

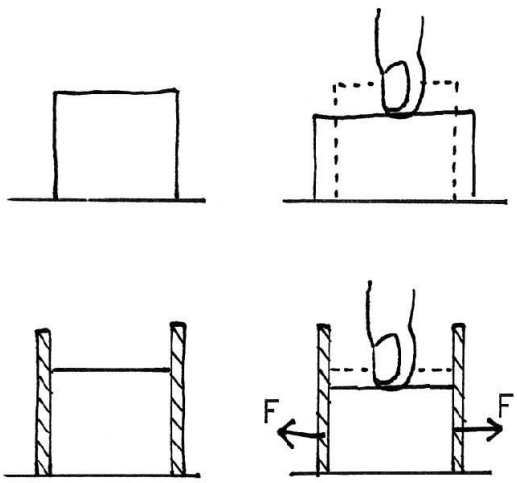


FIG. 2: Sketch of uniaxial compression of a free elastic material (top) and of a confined elastic material (bottom).

And the asymptotic displacements are

$$u_z(r,z) = -\frac{1+\nu_p}{2E}\rho g r^2 - \frac{1-\nu_p-2\nu_p^2}{2\mu_s\nu_p E}\rho g R z + u_0 \tag{12}$$

$$u_r(r,z) = u_\theta(r,z) = 0 \tag{13}$$

This can be checked by injecting this solution in the stress-strain relation (5) and internal equilibrium relation

$$\partial_i \sigma_{ij} = -\rho g_j \tag{14}$$

Thus, we obtain a Janssen's like redirection phenomenon due to a Poisson's ratio effect with a local Janssen's parameter $K_{el} = \sigma_{rr}(r,z)/\sigma_{zz}(r,z)$, being for large depths:

$$K_{el} = \frac{\nu_p}{1-\nu_p} \tag{15}$$

At 2D, we obtain the same saturation and stress redirection phenomena with $K_{el} = \nu_p$.

For a free elastic medium, the Poisson ratio effect is a transverse dilatation; for a confined elastic material, the Poisson ratio effect is a transverse redirection of stresses (Fig. 2).

In the following, K_{el} will design the elastic stress redirection constant, whereas K is devoted to design the stress redirection constant in the Janssen framework.

In this section, we obtained the asymptotic values of stresses and displacements. For the vertical stress, the limit is similar to the Janssen asymptotic vertical stress if one identifies K an K_{el}. But we cannot say anything from this calculation about the whole pressure profile. We thus need to perform numerical computation. In the next section, we present the numerical methods we employed to simulate Janssen experiments for an elastic column.

B. Numerical methods

Two different methods were employed: we first computed the stresses in 2D with a spring lattice. We also computed the stresses in 3D, using Finite Element Method thanks to CAST3M [24].

1. 2D: spring lattice

The 2D computations are performed in order to provide elastic predictions for a direct comparison with 2D simulations of granular materials.

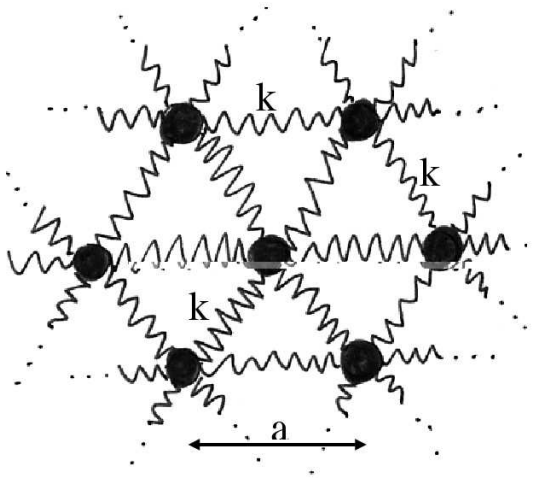


FIG. 3: Sketch of the discrete 2D elastic medium.

In order to avoid any confusion, let us recall that we are not trying here to give a microscopic model for a granular material, but we use a discrete system behaving like an effective elastic medium in the continuous limit in order to perform simple numerical simulations.

However, this system can describe the most simple of granular materials: a 2D hexagonal piling of frictionless disks (with non-hertzian contacts so that contact elasticity is linear). Note also that systems of springs have been recently studied by Goldenberg and Goldhirsch [25]; they showed that large forces inhomogeneities (i.e. like forces chains) can be found at the discrete scale in these systems, which are elastic in the continuous limit.

In order to simulate a 2D elastic medium, we put point masses m on an hexagonal lattice of link size a (Fig. 3). Every particle is linked to her 6 neighbors with identical springs of stiffness k and length a at rest. Therefore, the potential interaction energy between particles placed at 0 and x_i (such that $x_i x_i = a^2$) at rest, submitted to infinitesimal displacements u_i and v_i, is:

$$E_p = \frac{1}{2}k\Big(\sqrt{(x_i + v_i - u_i)(x_i + v_i - u_i)} - a\Big)^2 \tag{16}$$

By varying the stiffness k, we can only vary the young modulus E of the effective elastic medium. As we also need to vary the Poisson ratio ν, an elastic torsion potential between neighbor springs separated by angle θ (Fig. 4) is added:

$$E_p = \frac{1}{2}k_b \cos^2(\theta - \frac{\pi}{3}) \tag{17}$$

This potential tries to maintain an angle $\pi/3$ between 2 neighbors springs if $k_b < 0$. Thus the limit $k_b \to infty$ corresponds to a contractive medium of Poisson ratio -1, whereas the limit $k_b \to \infty$ corresponds to a incompressible medium.

An elementary area $A = a^2\sqrt{3}/2$ can be associated to each particle. The surface energy ω then reads:

$$\omega = \frac{2}{\sqrt{3}a^2}\left(\frac{1}{2}\sum E_p(springs) + \sum E_p(angles)\right) \tag{18}$$

If we consider the continuum limit of this system, the displacement of a particle located at x_i is:

$$u_i = (\partial_j u_i)x_j \tag{19}$$

The surface potential energy can be easily computed at second order in $\epsilon_{ij} = (1/2)(\partial_i u_j + \partial_j u_i)$, and one obtains:

$$\omega = \frac{\sqrt{3}}{2}\left(\frac{3}{4}(k + 2k_b)(\epsilon_{xx}^2 + \epsilon_{yy}^2) + \frac{1}{2}(k - 6k_b)\epsilon_{xx}\epsilon_{yy} + (k + 6k_b)\epsilon_{xy}^2\right) \tag{20}$$

For an elastic medium, stress-strain linearity reads

$$\sigma_{ij} = C_{ijkl}\epsilon_{kl} \tag{21}$$

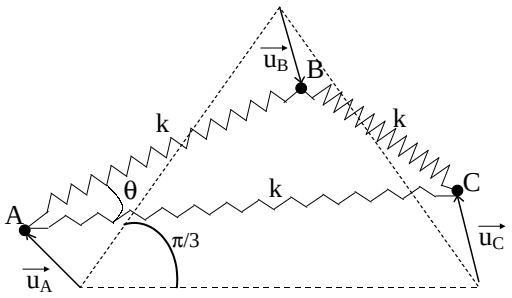


FIG. 4: Displacements of the points of an elementary cell of the 2D elastic medium.

There are *a priori* 9 independent parameters in C_{ijkl} (but only 2 if it is an isotropic elastic medium). The surface energy then reads

$$\omega = \frac{1}{2}\sigma_{ij}\epsilon_{ij} = \frac{1}{2}\epsilon_{ij}C_{ijkl}\epsilon_{kl} \tag{22}$$

If we identify this energy to the one we obtained for the spring lattice, we see that our system, in the continuous limit, is an isotropic elastic medium of Young modulus E and Poisson ratio ν_p:

$$\nu_p = \frac{1}{3}\frac{k-6k_b}{k+2k_b} \tag{23}$$

$$E = \frac{2\sqrt{3}}{3}k\frac{k+6k_b}{k+2k_b} \tag{24}$$

In order to solve the equilibrium problem of the lattice, we need to express the internal forces. They can be deduced from the surface energy (22): to the usual elastic forces due to compression (or decompression) of springs, add forces which tends to drive the triangles angles to their equilibrium value (if $k_b < 0$) or out of the $\pi/3$ value (if $k_b > 0$). The force on A, due to the out of equilibrium angles of triangle ABC (Fig. 4) reads:

$$F_{A_i} = -\frac{3}{2}k_b(u_{A_i} + R_{-\pi/3_{ij}}u_{B_j} + R_{\pi/3_{ij}}u_{C_j}) \tag{25}$$

where $R_{\theta_{ij}}$ is the rotation matrix of angle θ.

For the numerical computation, we impose the balance of forces (gravity, elastic forces, torsion forces) everywhere. At the bottom, we impose a null vertical displacement (rigid bottom), and either a perfectly stick (i.e. nullity of horizontal displacement) or perfectly slip (i.e. nullity of horizontal projection of forces) bottom. At the walls, we impose a null horizontal displacement (rigid wall), and we impose the Coulomb condition: the forces projected vertically are proportional to the forces projected horizontally with proportionality factor μ_s. On top of the material, the forces projected horizontally are null (perfectly slip overweight), and the overweight is simulated by imposing the same vertical displacement for each particle on top (stiff overweight), which is close to the experimental situation. We thus obtain a linear system on the point displacements. We can vary stiffness k and k_b in order to simulate elastic mediums of different Young modulus and Poisson ratio. Note that for varying ν_p between 0 and 1, we need to vary k_b between $-k/6$ and $k/6$. We also vary the friction at the walls μ_s.

2. 3D: FEM

In order to get the whole stress saturation curve, finite element numerical simulations [24] were performed. The column is modelled as an isotropic elastic medium. We vary the friction at the walls μ_s, the Young modulus E and the Poisson ratio ν_p. We imposed a rigid (nullity of vertical displacements), either perfectly stick (nullity of horizontal displacements) or perfectly slip (nullity of horizontal stresses) bottom. We found no appreciable difference between these two previous cases. The condition $\sigma_{rz} = \mu_s\sigma_{rr}$ is imposed everywhere at the walls. The cylinder is modelled as

a steel elastic medium. We verified that in all the simulations performed, there is no traction in the elastic medium, so that this can actually be a model for a granular material.

For the simulations performed without overweight, the top surface is set free (no stress); the overweight is modelled as a perfectly slip (no horizontal stress) brass elastic medium.

In order to impose the Coulomb condition at the walls, we first set $F_z = 0$ at each point of the mesh at the walls; we then obtain in these conditions the value F_r exerted by the elastic medium on the walls. We then iterate in order to obtain $F_z = \mu_s F_r$ where μ_s is the friction coefficient at the walls: the vertical force imposed at step (i+1) is:

$$F_z(i+1) = (1-\epsilon) \times F_z(i) + \epsilon \times \mu_s F_r(i) \tag{26}$$

We choose $\epsilon = 0.2$. This procedure ensures convergence towards the Coulomb condition: if at step (i) the Coulomb condition $F_z(i) = \mu_s F_r(i)$ is fulfilled, then at step (i+1): $F_z(i+1) = (1-\epsilon)F_z(i)+\epsilon\mu_s F_r(i) = (1-\epsilon)\mu_s F_r(i)+\epsilon\mu_s F_r(i) = \mu_s F_r(i) = F_z(i)$. This boundary condition is the same as the one at step (i): this yields $F_r(i+1) = F_r(i)$, and thus $F_z(i+1) = \mu_s F_r(i+1)$.

3. Remarks

Note that in these simulations we imposed the Coulomb condition everywhere at the walls. This allows comparison with the Janssen model in the same situation. But, regarding the experimental results [16], i) nothing really insures that our piling preparation is strictly isotropic and ii) in spite of the careful procedure, we are never absolutely sure that all the friction forces at the wall are actually mobilized upwards. Moreover, the modelling of the contacts may seem rudimentary, as elasticity of contact should be included.

In these simulations, imposing dynamical friction at the walls or the static Coulomb threshold is actually the same: the material obeys the same equilibrium equations (if we consider a steady sliding at the walls), and the same condition at the walls, with just a change in the name (and the experimental value) of the friction coefficient.

IV. SIMULATION RESULTS

In this section, we present the results obtained from numerical computations at 2D and 3D.

In the following, we vary mainly the friction coefficient, and the Poisson ratio. The 2D simulations are in arbitrary units. The 3D simulations were all performed, if no contrary mention, for an isotropic elastic medium of mass density $\rho = 1.6\ \mathrm{g\,cm^{-3}}$ (which corresponds to an assembly of glass beads of packing fraction $\bar{\nu} = 64\%$), of Young modulus 100 MPa, in a steel cylinder of radius $R = 4$ cm, Poisson ratio 0.3, Young modulus 210 GPa, and thickness 3 mm. These data, which correspond to the display used in [16], will not be specified anymore in the following. Simulations will also be performed in order to study the influence of the variation of the cylinder radius and the Young modulus of the elastic medium.

A. Simulations without overweight

We first perform simulations similar to the original Janssen experiment: we plot the weight at the bottom as a function of the weight of elastic material in the column (Fig. 5).

We see on Fig. 5, for friction coefficient $\mu_s = 0.5$ and Poisson ratio $\nu_p = 0.45$, that the apparent mass M_a saturates exponentially with the filling mass. The data are perfectly fitted by the Janssen model for these parameters (Fig. 5), but the Janssen coefficient K extracted from the fit is 9% higher than the elastic stress redirection constant $K_{el} = \nu_p/(1-\nu_p) = 0.82$. This is *a priori* unexpected as the elastic saturation pressure and the Janssen one should be identical with $K = K_{el}$.

1. Effect of the bottom

In order to understand this feature, we study the whole mean vertical pressure profile in the same column (Fig. 6).

Regarding mean vertical pressure, we see that the asymptotic value is now the expected theoretical asymptotic value, and the Janssen curve with $K = K_{el}$ gives a good though not perfect fit of the profile. The pressure saturates at high depths but decreases suddenly near the bottom; this is actually the value on the bottom we measure in a Janssen experiment. This feature explains why the saturation mass is lower than the expected one on Fig. 5. The

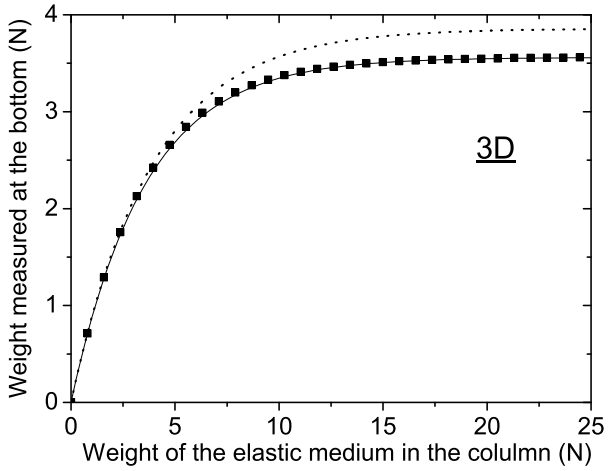


FIG. 5: 3D simulation of a Janssen experiment (squares) for an elastic material of Poisson ratio $\nu_p = 0.45$; the friction at the walls is $\mu_s = 0.5$. The data are fitted by a Janssen curve of coefficient $K = 0.89$ (line). The Janssen curve for K corresponding to the elastic stress redirection constant $K_{el} = \nu_p/(1-\nu_p) = 0.82$ is also displayed (dotted line).

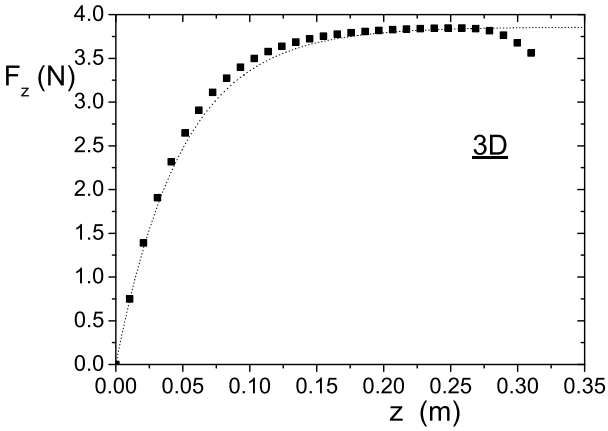


FIG. 6: Mean pressure profile in a simulated elastic material of height 31 cm and Poisson ratio $\nu_p = 0.45$ (squares); the friction at the walls is $\mu_s = 0.5$. Depth $z = 0$ cm corresponds to the top of the column. Depth $z = 31$ cm corresponds to the bottom. We display the integral of vertical stresses F_z at height z. The data are compared to a Janssen curve of coefficient $K = K_{el} = 0.82$ corresponding to the elastic stress redirection constant (dotted line).

reason for this change of pressure near the bottom is that the asymptotic vertical displacement is parabolic whereas the bottom is rigid and imposes a flat displacement.

It is thus important to note that the usual Janssen experiment, in which one measure is made for one given height, is not equivalent to measuring a pressure profile, and results in a lower saturation stress (i.e. higher Janssen's constant K) than the pressure profile. For more clarity on this last point, we illustrate this difference on Fig. 7.

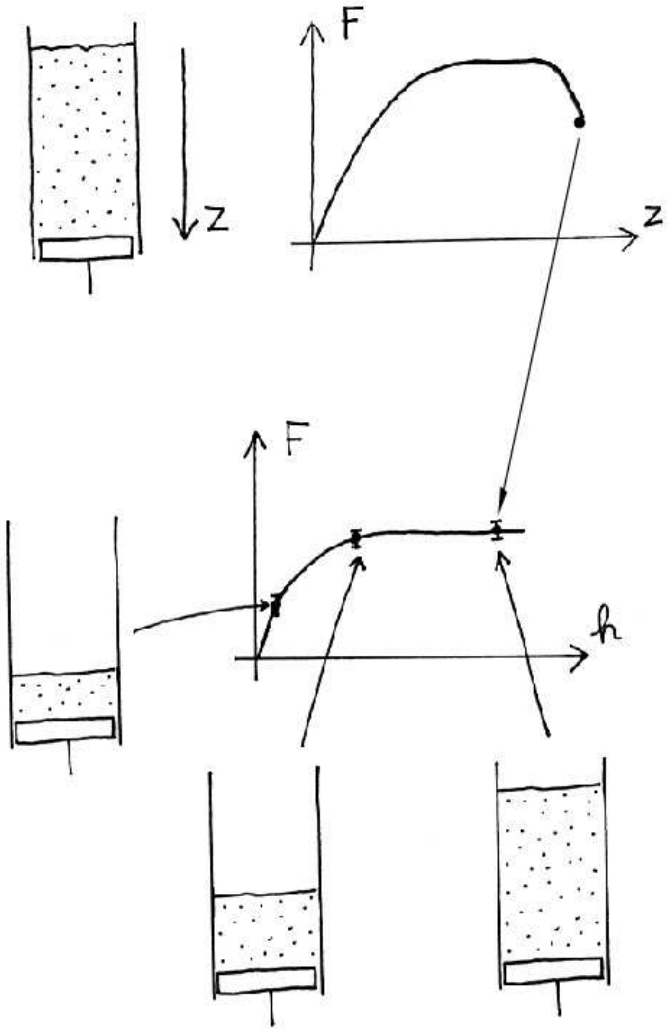


FIG. 7: Sketch of comparison between a pressure profile and measures at the bottom for an elastic medium.

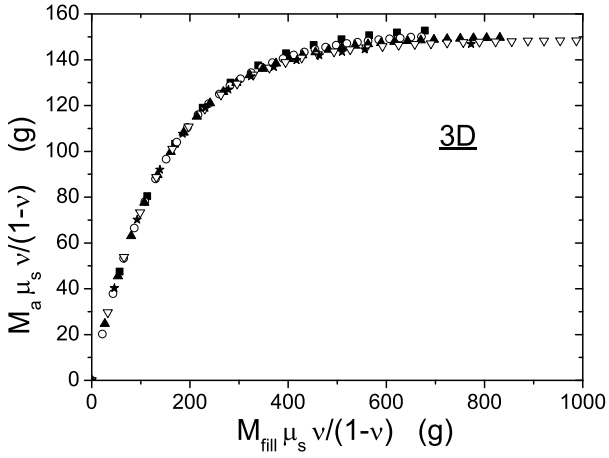


FIG. 8: Study of the rescaling with the Poisson ratio ν_p for 3D simulations of an elastic material. We plot $M_a \times \mu_s \nu_p/(1-\nu_p)$ vs. $M_{fill} \times \mu_s \nu_p/(1-\nu_p)$ for $\nu_p = 0.26$ (squares), $\nu_p = 0.35$ (open circles), $\nu_p = 0.4$ (triangles), $\nu_p = 0.45$ (open down triangles) and $\nu_p = 0.49$ (stars); the friction at the walls is $\mu_s = 0.5$.

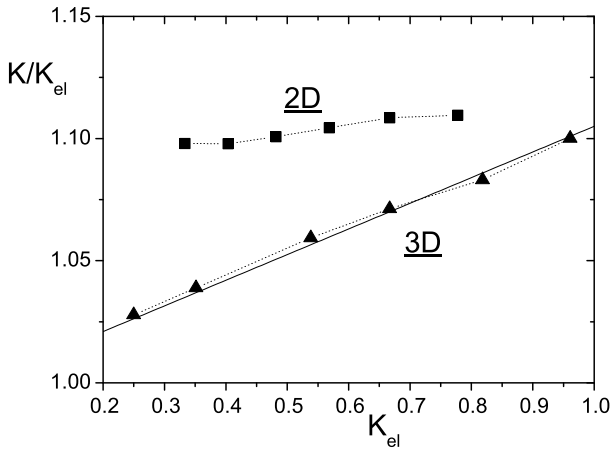


FIG. 9: Janssen constant K extracted form 2D (squares) and 3D (triangles) simulations for various Poisson ratios. In the 2D simulations, the friction at the walls is $\mu_s = 1.0$; in the 3D simulations, the friction at the walls is $\mu_s = 0.5$. K is plotted vs. the elastic stress redirection constant $K_{el} = \nu_p$ in 2D, $K_{el} = \nu_p/(1-\nu_p)$ in 3D.

In the following, we study the rescaling law of simulated Janssen experiments with friction coefficient μ_s at the walls and the Poisson ratio ν_p. The data are compared to the Janssen model predictions by plotting $M_a \times \mu_s \times \nu_p/(1-\nu_p) = f(M_{fill} \times \mu_s \times \nu_p/(1-\nu_p))$ for different μ_s and ν_p (since $K_{el} = \nu_p/(1-\nu_p)$ and $M_{sat} \propto 1/(K_{el}\mu_s)$).

2. Effect of the Poisson ratio

On Fig. 8, we study the rescaling with the Poisson ratio ν_p for 3D simulations. The rescaling law is rather good, the differences may not be observable experimentally. On Fig. 9 we plot the Janssen coefficient K extracted from the fit of data in 2D and 3D versus the elastic stress redirection constants K_{el} (ν_p in 2D, $\nu_p/(1-\nu_p)$ in 3D).

We observe that for a given friction coefficient, K hardly depends on ν_p in 2D: K variation is 1% for K_{el} varying from 0.33 to 0.77. In 3D, K/K_{el} increases roughly linearly with K_{el} for K_{el} varying from 0.25 to 0.96; however, K variation is less than 10% in this range. We remark that $K > K_{el}$: we explained it in the preceding section as a consequence of the presence of the rigid bottom.

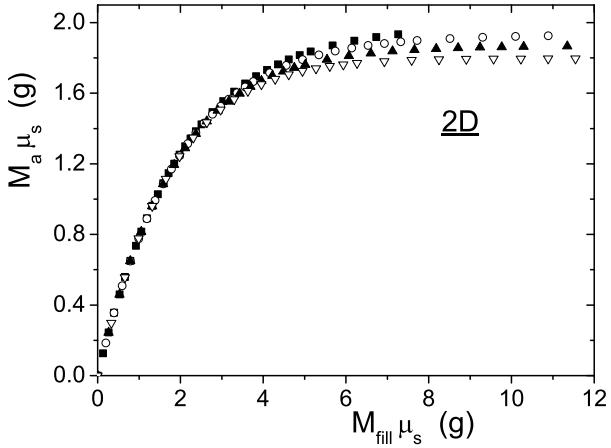


FIG. 10: Study of the rescaling with the friction coefficient μ_s at the walls for 2D simulations of an elastic material. We plot $M_a \times \mu_s$ vs. $M_{fill} \times \mu_s$ for $\mu_s = 0.4$ (squares), $\mu_s = 0.6$ (open circles), $\mu_s = 0.8$ (triangles) and $\mu_s = 1.0$ (open down triangles); the Poisson ratio is $\nu_p = 0.77$.

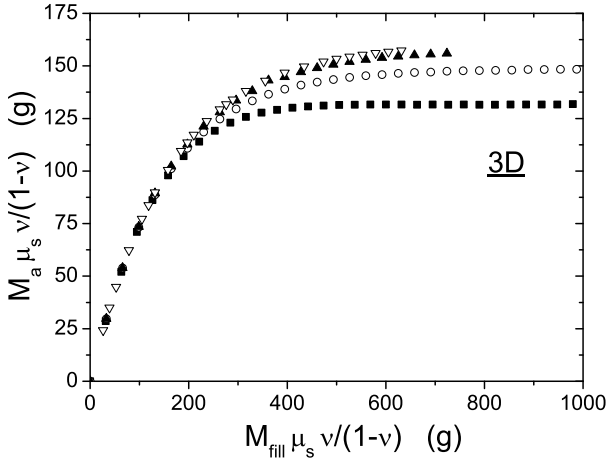


FIG. 11: Study of the rescaling with the friction coefficient μ_s at the walls for 3D simulations of an elastic material. We plot $M_a \times \mu_s \nu_p/(1-\nu_p)$ vs. $M_{fill} \times \mu_s \nu_p/(1-\nu_p)$ for $\mu_s = 0.1$ (open down triangles) $\mu_s = 0.25$ (triangles), $\mu_s = 0.5$ (open circles) and $\mu_s = 0.8$ (squares); the Poisson ratio is $\nu_p = 0.45$.

3. Effect of friction at the walls

On Fig. 10 and Fig. 11, we study the rescaling with the friction coefficient μ_s at the walls respectively for 2D and 3D simulations. We now see that the proposed rescaling law is not good: the saturation is more abrupt as the friction coefficient is higher.

On Fig. 12 we plot the Janssen coefficient K extracted from the saturation mass value in 2D and 3D versus μ_s. We now observe that the Janssen constant (and thus the saturation mass) depends strongly on the friction coefficient at the walls: K increase is 12% in 2D for μ_s varying between 0.1 and 1.0, and 20% in 3D for μ_s varying from 0.1 to 0.8. K depends roughly quadratically on μ_s. Moreover, the Janssen constant seems to tend towards the elastic stress redirection constant K_{el} when μ_s goes to 0.

In order to understand these features, we plot on Fig. 13 the mean vertical pressure F_z versus the depth, and its rescaling with μ_s.

We see that, regarding the pressure profile, the Janssen rescaling law is correct for the asymptotic value, but the profiles are slightly different: for low friction at the walls $\mu_s \approx 0.25$, the profile is perfectly fitted by the Janssen law; for higher friction, the profile is sharper and saturates abruptly. The differences for simulated Janssen experiments observed on Fig. 11 are now identified as a consequence of the presence of a rigid bottom: we actually see on Fig. 13 that the decrease of pressure near the bottom is more important when the friction is higher i.e. the saturation mass is lower (and the effective Janssen constant is higher).

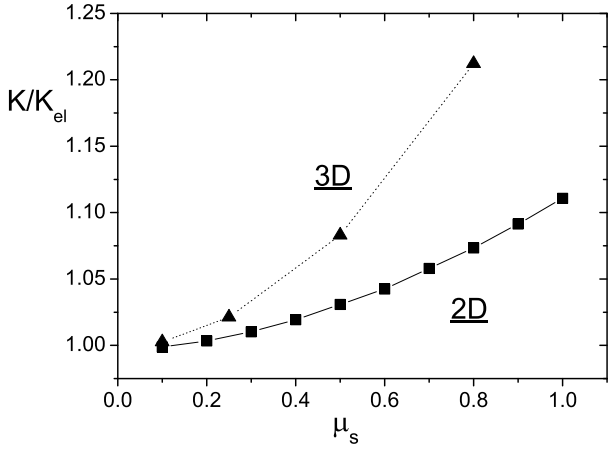


FIG. 12: Janssen constant K extracted form 2D (squares) and 3D (triangles) simulations for various friction coefficient μ_s. In the 2D simulations, the Poisson ratio is $\nu_p = 0.77$; in the 2D simulations, the Poisson ratio is $\nu_p = 0.45$. K is rescaled by the elastic stress redirection constant $K_{el} = 0.77$ in 2D, $K_{el} = 0.82$ in 3D.

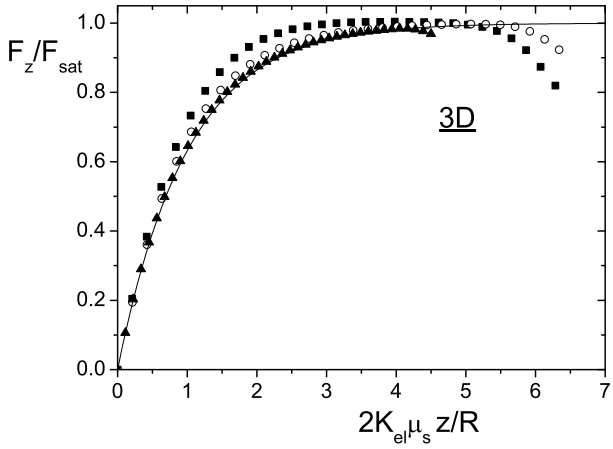


FIG. 13: Integral of vertical stresses F_z vs. depth z, for elastic materials of Poisson ratio $\nu_p = 0.45$, and friction at the walls $\mu_s = 0.25$ (triangles), $\mu_s = 0.5$ (open circles), et $\mu_s = 0.8$ (squares). We plot F_z/F_{sat} vs. $2K_{el}\mu_s\, z/R$ where $F_{sat} = \rho g \pi R^3/(2K_{el}\mu_s)$ is the theoretical saturation value for F_z. $z/R = 0$ corresponds to the top of the material. We also plot the Janssen model prediction with $K = K_{el} = \nu_p/(1-\nu_p)$ (line).

We now understand all these features: the parabolic part of asymptotic displacements is negligible for low friction; in this case, the flat displacement imposed by the rigid bottom matches the asymptotic displacement, and the pressure at the bottom is the saturation pressure: we thus obtain $K = K_{el}$. As the friction is increased (and the material leans on the walls), the parabolic part of asymptotic displacement becomes more important and the influence of the rigid bottom is to decrease pressure; we thus observe an increase in the effective Janssen constant K with μ_s.

4. A unique parameter

In the Janssen picture, the Janssen coefficient K and the friction at the walls μ_s are not independent parameters: the relevant parameter is $K\mu_s$. As regards the saturation mass M_{sat}, it remains true in elasticity, and we see on Fig. 14 that $K\mu_s$, extracted from the saturation mass value, is a function of $K_{el}\mu_s$ alone (i.e. data on Fig. 9 and 12 can be replotted on a single universal curve); we find a quadratic dependence of $K\mu_s$ on $K_{el}\mu_s$: $K\mu_s \approx K_{el}\mu_s + 0.29(K_{el}\mu_s)^2$. This explains the dependence found before on ν_p at fixed μ_s or on μ_s at fixed ν_p.

However, it is not true anymore for the whole Janssen profile: we see on Fig. 15 that there is not a universal curve $M_a/M_{sat} = f(M_{fill}/M_{sat})$: if most data may be fit by the Janssen curve (with $f(x) = 1 - \exp(-x)$, it is not true anymore for high (i.e. low M_{sat} values); the data for high values of $K\mu_s$ (=0.65 here) fall above the Janssen curve.

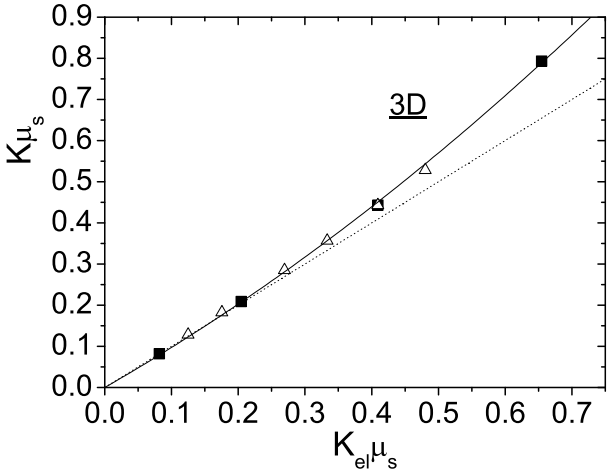


FIG. 14: Janssen constant K extracted form 3D (triangles) simulations for various friction coefficient μ_s at constant $\nu_p = 0.45$ (empty triangles) and various Poisson ratios ν_p at constant $\mu_s = 0.5$ (squares); see Fig. 8 and 11 for ν_p and μ_s values. The dotted line is the $y = x$ line; the line is a polynomial fit with $K\mu_s = K_{el}\mu_s + 0.29(K_{el}\mu_s)^2$.

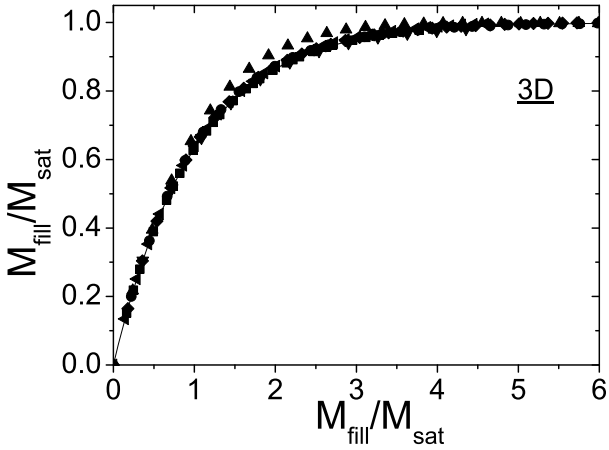


FIG. 15: M_a/M_{sat} vs. M_{fill}/M_{sat} for 3D simulations for various values of ν_p and μ_s; the triangles are for $\nu_p = 0.45$ and $\mu_s = 0.8$.

However, for most experimental conditions, $K\mu_s$ is not as high, and this effect will not be observable.

5. Effect of walls elasticity

On Fig. 16, the Young modulus is varied.

We observe that the results are independent of the Young modulus E value, as long as it is less than 500 MPa; we see on Fig. 16 that the curves obtained for the simulation of a Janssen experiment for $E = 1$ MPa and $E = 200$ MPa can be perfectly superposed. For higher E, the weighted mass is higher and does not seem to saturate anymore; as an example, for $E = 4$ GPa on Fig. 16, M_a seems to increase indefinitely.

Note that this Young modulus effect is present only because we take into account the walls elasticity; for rigid walls and bottom, there would not be any dependence on E. The values of E presented here have a meaning only for a particular cylinder (same E and same thickness).

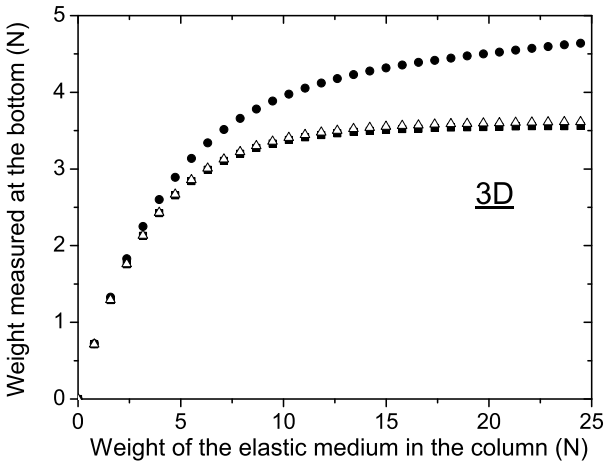


FIG. 16: Simulation of a Janssen experiment for elastic materials of Young modulus $E = 1$ MPa (squares), $E = 200$ MPa (open triangles) et $E = 4$ GPa (circles), of Poisson ratio $\nu_p = 0.45$, in a steel column of radius $R = 4$ cm; the friction coefficient at the walls is $\mu_s = 0.5$.

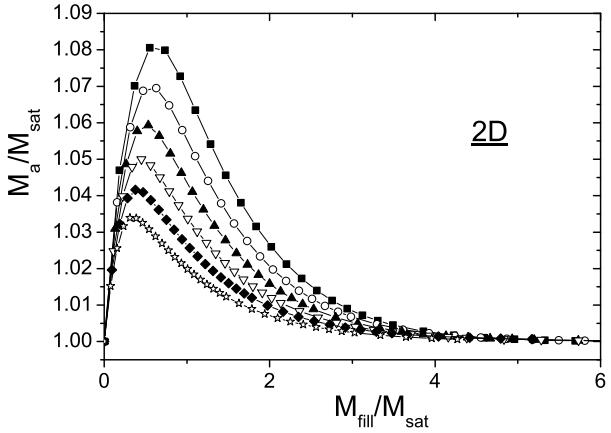


FIG. 17: Weight at the bottom of a 2D elastic material, when an overweight equal to the saturation mass is added on top of the material, for various Poisson ratio ν_p: 0.33 (open stars), 0.40 (diamonds), 0.48 (open down triangles), 0.57 (triangles), 0.67 (open circles) and 0.78 (squares). The friction coefficient at the walls is $\mu_s = 1.0$. The data are scaled with the saturation mass obtained in a simulation without overweight.

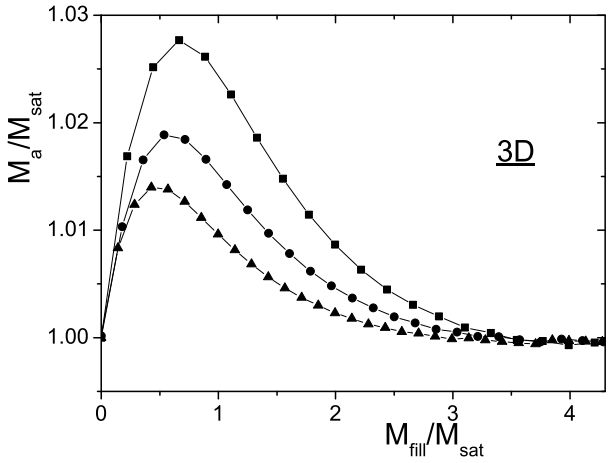


FIG. 18: Weight at the bottom of a 3D elastic material, when an overweight equal to the saturation mass is added on top of the material, for Poisson ratio $\nu_p = 0.35$ (triangles), $\nu_p = 0.4$ (circles) et $\nu_p = 0.45$ (squares). The friction coefficient at the walls is $\mu_s = 0.5$. The data are scaled with the saturation mass obtained in a simulation without overweight.

B. Simulations with an overweight

In this section, we present simulations of a Janssen experiment, when an overweight corresponding to the saturation mass is added on top of the material.

1. Effect of the Poisson ratio

On Fig. 17 and 18, we plot the apparent mass M_a versus the filling mass M_{fill}, rescaled by the saturation mass M_{sat}, respectively in 2D and 3D, for various Poisson ratio.

We now observe that, contrary to the simulations without any overweight, the results depend strongly on ν_p, i.e. on the elastic stress redirection constant K_{el}. The curves all have the same form: M_a increases with M_{fill}, up to a maximum M_{max}, then decreases slowly towards the saturation mass M_{sat}. The relative maximum M_{max}/M_{sat} increase with ν_p, and takes its value for higher M_{fill}/M_{sat}.

The proposed rescaling law, similar to the Janssen one, is not correct. We did not find any rescaling law; we thus keep our rescaling as a practical representation of data.

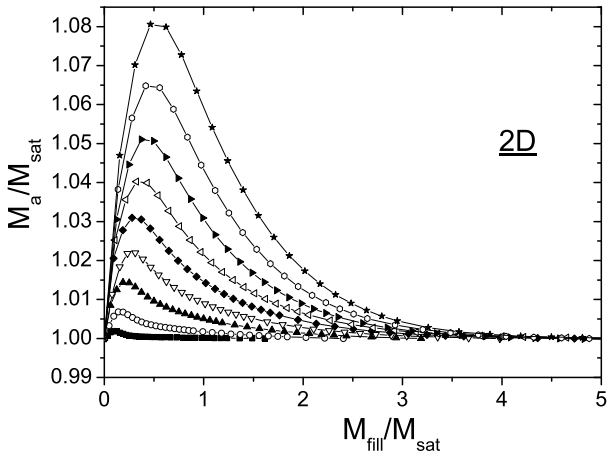


FIG. 19: Weight at the bottom of a 2D elastic material, when an overweight equal to the saturation mass is added on top of the material, for various friction coefficients μ_s: 0.2 (squares),0.3 (open circles)), 0.4 (triangles), 0.5 (open down triangles), 0.6 (diamonds), 0.7 (open left triangles), 0.8 (right triangles), 0.9 (open hexagons) and 1.0 (stars). The Poisson ratio is $\nu_p = 0.78$. The data are scaled with the saturation mass obtained in a simulation without overweight.

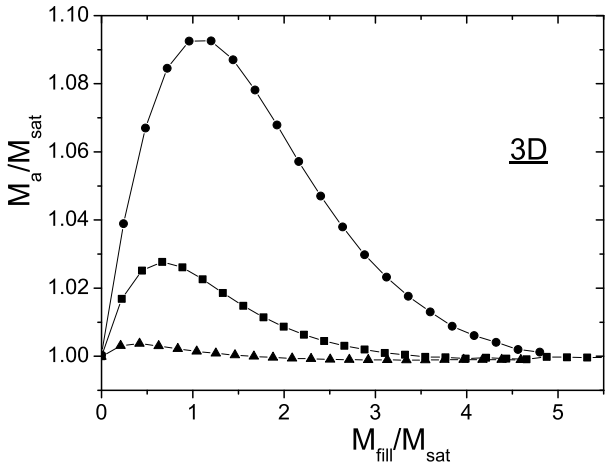


FIG. 20: Weight at the bottom of a 3D elastic material, when an overweight equal to the saturation mass is added on top of the material, pour friction coefficient $\mu_s = 0.25$ (triangles), $\mu_s = 0.5$ (squares) and $\mu_s = 0.8$ (circles). The Poisson ratio is $\nu_p = 0.45$. he data are scaled with the saturation mass obtained in a simulation without overweight.

2. Effect of friction at the walls

On Fig. 19 et 20, we plot the apparent mass M_a versus the filling mass M_{fill}, rescaled by the saturation mass M_{sat}, respectively in 2D and 3D, for various friction coefficients at the walls.

We observe that the relative maximum of the apparent mass M_{max}/M_{sat} increases with the friction coefficient at the walls, and takes its value for higher M_{fill}/M_{sat}.

This result leads to an apparent paradox. As actually the maximum M_{max} increases when M_{sat} decreases (i.e. when μ_s and ν_p increase), we observe that *the more the weight of the grains is screened by the walls, the less the weight of the overload is screened*! We will propose an interpretation in the following.

3. Study of the pressure profile

We can wonder if all these results remain true for the profile. These features could be due only to the presence of a bottom. On Fig. 21, we plot the mean pressure profile when an overweight of mass equal to the saturation mass obtained in the simulation of a Janssen experiment is added on top of the material.

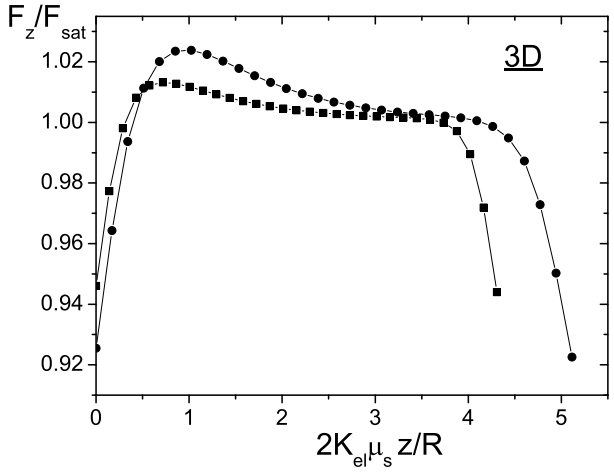


FIG. 21: Integral of vertical stresses F_z vs. depth z, for elastic materials of friction coefficient at the walls $\mu_s = 0.5$, and Poisson ratios $\nu_p = 0.35$ (squares) and $\nu_p = 0.45$ (circles), when an overweight equal to the saturation mass is added on top of the material. We plot F_z/F_{sat} vs. $K_{el}\mu_s\, z/R$ where $F_{sat} = \rho g \pi R^3/(2K_{el}\mu_s)$ is the theoretical saturation value for F_z. $z/R = 0$ corresponds to the top of the material.

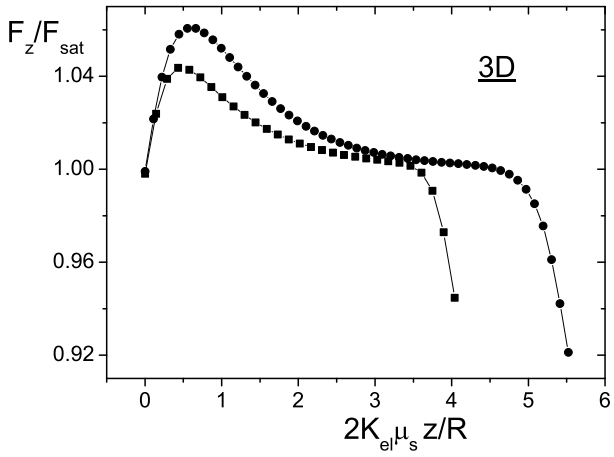


FIG. 22: Integral of vertical stresses F_z vs. depth z, for elastic materials of friction coefficient at the walls $\mu_s = 0.5$, and Poisson ratios $\nu_p = 0.35$ (squares) and $\nu_p = 0.45$ (circles), when an overweight equal to the saturation value F_{sat} of F_z. We plot F_z/F_{sat} vs. $K_{el}\mu_s\, z/R$ where $F_{sat} = \rho g \pi R^3/(2K_{el}\mu_s)$ is the theoretical saturation value for F_z. $z/R = 0$ corresponds to the top of the material.

We observe the same features as for the simulation of a Janssen experiment. In order to go one step further, we now add an overweight which imposes on top of the material a mean pressure equal to the saturation pressure; the results are presented on Fig. 22.

Once again, we observe the same features as for the simulation of a Janssen experiment. The Janssen rescaling law is still incorrect, and the overshoot effect is more important for higher Poisson ratio and friction coefficient. Moreover, on the profile the amplitude of the maximum is more important: for friction coefficient $\mu_s = 0.5$ and Poisson ratio $\nu_p = 0.45$, we find that the maximum force on the profile is 1.06 times the saturation force F_{sat}, whereas the maximum weighted mass is 1.03 times the saturation mass M_{sat}.

4. Rescaling with the radius

We finally verify the rescaling with the radius column for simulations with and without any overweight. This rescaling is perfect for both simulations (Fig. 23) for the extreme radius employed in [16] ($R = 1.9$ cm et $R = 4$ cm).

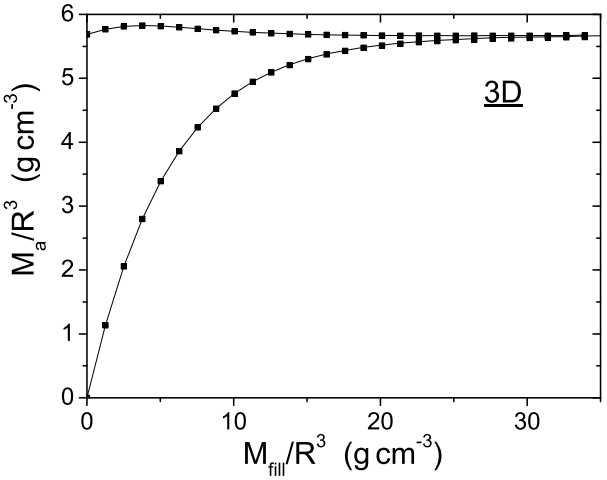


FIG. 23: Study of the rescaling with the radius R of the column. We plot M_a/R^3 vs. M_{fill}/R^3 for $R = 1.9$ cm (squares) et $R = 4$ cm (line), for an elastic material of Poisson ratio $\nu_p = 0.45$ and friction coefficient at the walls $\mu_s = 0.5$.

C. Observable features

To summarize, several features are experimentally observable if the isotropic elastic theory is valid.

In a Janssen experiment with free top surface, for a same material, the Janssen constant K, deduced from the measured saturation mass M_{sat}, must be higher for higher friction coefficient at the walls.

In an experiment with M_{sat} overweight on top of the material, the apparent mass M_a must increase strongly with the filling mass M_{fill}, and then decrease slowly towards the saturation mass M_{sat}. The observed maximum M_{max} must increase with friction at the walls and with Janssen coefficient K (measured in a Janssen experiment with free top surface).

The saturation mass M_{sat} deduced from the pressure profile must be higher than the one measured at the bottom, and a strong decrease in the pressure must be observed near the bottom. This kind of feature would not be observed for a hyperbolic theory such as OSL [7]. Moreover, for experiments with an overweight on top of the material, the maximum of M_a will be higher on the pressure profile.

D. Comparison with experimental results

In this section, we compare the elastic theory predictions to the experimental results obtained in [16]. The main features have already been presented in [16]

1. Classical Janssen experiment

The Janssen experiment data are perfectly fitted by the Janssen model. Therefore, they are also perfectly fitted by the elastic theory: we indeed showed in Sec. IV A that for weak friction at the wall ($\mu_s = 0.25$ as in the experiment) the Janssen model and elastic theory predictions cannot be discerned.

We also showed in Sec. IV A 3 that when the friction coefficient is increased, the elastic theory predict a sharper initial increase of M_a with M_{fill} and an more abrupt saturation. However, this cannot be observed experimentally for the small range of friction coefficient used in [16] (from 0.22 to 0.28). In order to test this last prediction, it would be necessary to work with higher friction at the walls ($\mu_s \sim 0.5$).

Note that for high packing fractions ($\nu = 0.645 \pm 0.005$), we obtained Janssen coefficients higher than 1 ($K = 1.2 \pm 0.1$): this cannot be obtained in the isotropic elastic theory, as $K_{el} = \nu_p/(1-\nu_p) \leq 1$. We saw that K_{el} is less than K (Fig. 9, 12), due to presence of a rigid bottom, but for small friction at the walls, this cannot explain high K values: we deduce from Fig. 12 that for $\mu_s = 0.25$, K must be less than 1.03; for $\mu_s = 0.8$, K could be as high as 1.2. We will see in Sec. IV I how to obtain higher K values in the context of anisotropic elasticity.

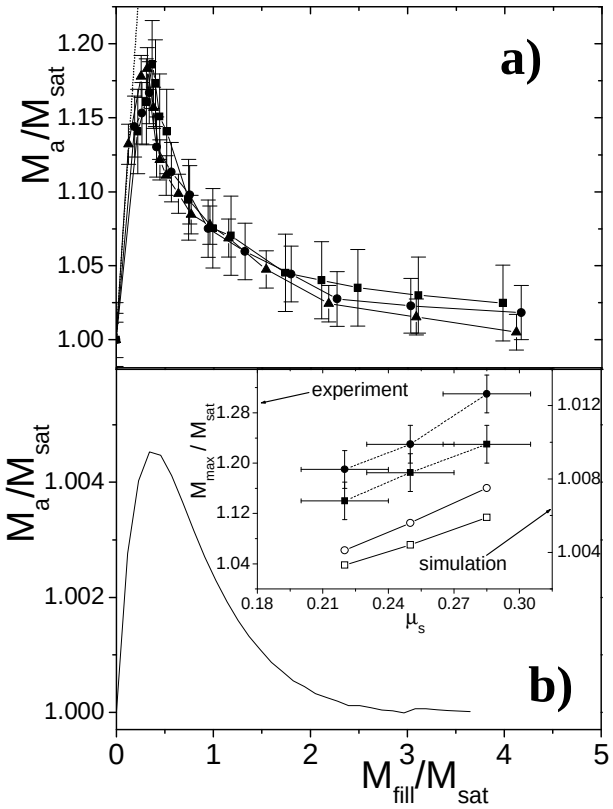


FIG. 24: a: Apparent mass M_a vs. filling mass M_{fill}, rescaled by the saturation mass M_{sat}, for loose packing in medium-rough columns of 3 diameters (38 mm (squares), 56 mm (circles), 80 mm (triangles)) with an overweight equal to M_{sat}; the dotted line is the hydrostatic curve. b: Simulation of the experiment of Fig. 24a, for an elastic medium characterized by the same saturation mass (Poisson ratio $\nu_p = 0.46$) and the same friction at the walls ($\mu_s = 0.25$). Inset: maximum mass M_{max} rescaled by saturation mass M_{sat} vs. static coefficient of friction at the walls μ_s, in experiments made on loose (squares) and dense (circles) packing in 38 mm diameter columns, and in simulations for elastic media of Poisson ratios $\nu_p = 0.45$ (open squares) and $\nu_p = 0.49$ (open circles); the left vertical scale is used for the experimental data, the right vertical scale is used for the simulation data.

It was observed in [16] that for different preparations, characterized by different packing fractions, the saturation mass M_{sat} is lower for higher packing fraction. Although there may be structural differences between the pilings other than the packing fraction, this can be interpreted as increase of the Janssen coefficient K with packing fraction. Thus, in the context of isotropic elasticity, this leads to an effective increase of the Poisson ratio ν_p with packing fraction. In [16], an effective relation between packing fraction $\bar{\nu}$ and Poisson ratio ν_p was derived: $\nu_p \simeq 2.3(\nu - 0.41)$ with a precision of 5%. Note that the largest packing fraction $\nu = 0.645 \pm 0.005$ would give a Poisson ratio $\nu_p = 0.54 \pm 0.03$ marginally larger than the limit value of 1/2, as commented above.

2. Overweight experiment

The elastic theory gives qualitatively the same behavior as the experimental results (see Fig. 24): the apparent mass M_a increases with the filling mass M_{fill}, up to a maximum M_{max}, then decreases slowly towards the saturation mass M_{sat}. Furthermore, all the features predicted by elasticity can be observed: R^3 rescaling, M_{max}/M_{sat} increase with friction at the walls, and M_{max}/M_{sat} increase with packing fraction (experiment) or Poisson ratio (theory). Note that M_{max}/M_{sat} increases with packing fraction and Poisson ratio are equivalent because of the effective increase of Poisson ratio with packing fraction deduced from the classical Janssen experiment.

However, there is no quantitative agreement between isotropic elasticity predictions and experiments. Fig. 24). The elastic curve is very similar to the experimental one, but the experimentally observed maxima are 30 to 40 times larger.

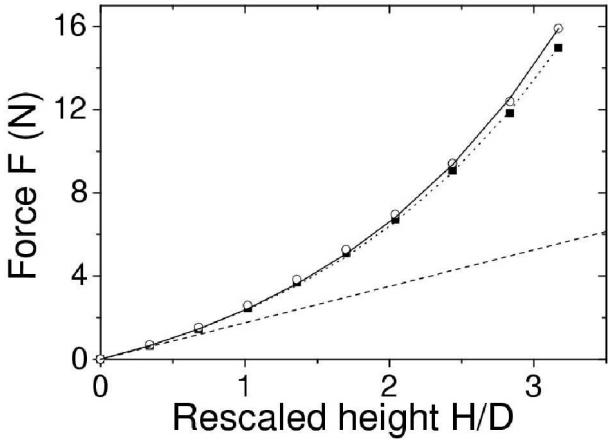


FIG. 25: Mean resistance force to pushing as a function of the height H of the packing scaled by the column diameter D, for 1.58 mm steel beads, of packing fraction 62.5%, in a 36 mm duralumin column, for $V = 16\ \mu\mathrm{m\,s}^{-1}$ (filled squares) and $V = 100\ \mu\mathrm{m\,s}^{-1}$ (open circles). The line and the dotted line are fits by eq. (28). The dashed line is the hydrostatic curve.

E. An apparent paradox explained by elasticity

Interestingly, we find in the elastic case the same qualitative phenomenology as in the experiment i.e. the computed values of the overshoot M max rescaled by the saturation mass M_{sat} increases both with the friction at the walls and the Poisson coefficient (i.e. with the effective Janssen's parameter). This features reads as a paradox: *the more the weight of the grains is screened by the walls, the less the weight of the overload is screened*, but we can now try to understand it at least qualitatively.

If we impose on the top surface of an elastic medium the asymptotic values for displacements and stresses (see eq. (11), (12)), these values then extend to the rest of the column. Thus, with such an overweight, a flat pressure profile along depth z $\sigma_{zz}(r,z) = -\frac{\rho g R}{2K_{el}\mu_s}$ is obtained as in Janssen's theory. Actually, with the overload, the displacement imposed experimentally on the surface is almost constant: $u_z(r) = u_0$ since the overweight is much more rigid than the material. Then, as the asymptotic displacement is parabolic, we must have a "transition regime", which is at the origin of the overshoot effect.

There are two limits in which this transition can disappear, i.e. when the Poisson coefficient ν or when friction at the walls μ_s are decreased to zero. Then the parabolic part of the asymptotic displacements (eq. (12)) becomes negligible and therefore, the imposed displacement on the surface is close to the asymptotic value. This results in a decrease of the overshoot amplitude.

Basically, we thus recover in the elastic case, the same paradox as the experimental situation. We now understand it as a consequence of the boundary condition imposed experimentally by the overweight i.e. an almost constant displacement on the surface.

It would be interesting to put overweights of different Young modulus on top of a granular material in order to see if the overshoot amplitude decreases when the overweight Young modulus is decreased.

F. Pushing experiment

In this section, we study the elastic theory predictions for the force needed to push an elastic material upwards at constant velocity in a column, and compare it to recent experimental observations [14, 15] in the case of a slowly driven granular material. The main features of this analysis have been presented in [15].

For a vertically pushed granular assembly [14, 15] at constant velocity, the resistance force $\bar{F}$ increases very rapidly with the packing's height H(see Fig. 25).

Following the standard Janssen screening picture, this strong resistance to motion is due to the leaning of the granular material on the walls (eq. (4)) in association with solid friction at the side walls. At the walls, we suppose a sliding of the granular material at a velocity V_0 (the driving velocity); the shearing stress is then

$$\sigma_{rz}(z) = -\mu_d(V_0)\sigma_{rr}(z) \tag{27}$$

where $\mu_d(V_0)$ is the dynamic coefficient of friction between the beads and the cylinder's wall at a velocity V_0.

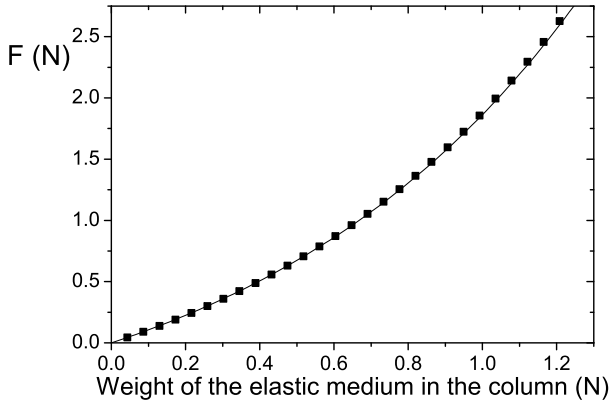


FIG. 26: Comparison of the resistance force to pushing simulated for a homogeneous isotropic elastic medium (squares) of Poisson ratio $\nu = 0.45$ and Young modulus $E = 100$ MPa in a duralumin cylinder of radius $R = 1.9$ cm, with coefficient of friction $\mu_d = 0.2$ at the walls, to the curve obtained with eq. (28) with Janssen coefficient $K = K_{el} = \nu/(1-\nu) = 0.82$ (line).

The force $\bar{F}$ exerted by the grains on the piston can be derived from equilibrium equations for all slices, thus we obtain:

$$\bar{F} = \varrho g \lambda \pi R^2 \times (\exp(\frac{H}{\lambda}) - 1) \tag{28}$$

where ϱ is the mass density of the granular material, R is the cylinder radius and g the acceleration of gravity. The length $\lambda = R/2K\mu_d(V_0)$ is the effective screening length.

We see on Fig. 25 that the data are well fitted by eq. (28). We obtain $K\mu_d(V) = 0.140 \pm 0.001$ at $V = 100\ \mu\mathrm{m\,s^{-1}}$ and $K\mu_d(V) = 0.146 \pm 0.001$ at $V = 100\ \mu\mathrm{m\,s^{-1}}$.

In order to get the isotropic homogeneous elasticity prediction for the pushing experiment, we perform a series of numerical simulations using Finite Element Method [24]. The condition $\sigma_{rz} = -\mu_d \sigma_{rr}$ is now imposed everywhere at the walls (for the pulling situation, we impose $\sigma_{rz} = +\mu_d \sigma_{rr}$). The cylinder is modelled as a duralumin elastic medium. As long as the Young modulus E of the elastic medium is less than 500 MPa, which is usually the case for granular media, we find no dependence of the results on E.

We find no appreciable difference between the elastic prediction (Fig. 26) and the curve given by eq. (28) with $K = K_{el}$. Therefore, regarding the dependence of the stationary state force $\bar{F}$ on the height of beads, our system cannot be distinguished from an elastic medium.

G. Pushing vs. pulling

As a check of consistency, we performed the following dynamical experiment in [15]. First, the granular column is pushed upwards in order to mobilize the friction forces downwards and far enough to reach the steady state compacity. Starting from this situation, the friction forces at the walls are reversed by moving the piston downwards at a constant velocity $V_{down} = 16\ \mu\mathrm{m\,s^{-1}}$, until a stationary regime is attained. Note that this stationary regime is characterized by the same compacity $\bar{\nu} \approx 62.5\%$ as in the pushing situation. In Fig. 27 the pushing force $\bar{F}$ is measured for different packing heights H. The fit of experimental results with eq. (2) gives $K\mu_d(16\ \mu\mathrm{m\,s^{-1}}) = 0.156 \pm 0.002$ which is 10% larger than $K\mu_d(16\ \mu\mathrm{m\,s^{-1}})$ extracted from the pushing experiment. This difference, though small, can be observed out of uncertainties, and is systematic. It cannot be due to a slight change in compacity $\bar{\nu}$ as from relation $\Delta K/K \approx 5\Delta\bar{\nu}/\bar{\nu}$, we would expect a 2% variation in compacity between the pushing and the pulling experiment, which would be observed; we actually measured $\Delta\bar{\nu}/\bar{\nu} = 0 \pm 1\%$. According to Janssen's picture, this would imply that vertical stress redirection is more efficient in the downward pulling situation. We believe this is a clear evidence of a granular structuring effects but its also shows that this effect is not dominant: it affects only 10% of the average mechanical parameter K.

Note that finite element simulations show that the presence of a rigid bottom implies that the effective Janssen's parameter K_{eff} extracted from Janssen's rescaling for the pulling situation is higher than K_{el}, whereas for the pushing $K_{eff} \approx K_{el}$ (as can be seen on Fig. 26: the fit of the elastic curve with $K = K_{el}$ is good). Actually, if we adjust the elastic predictions for pushing and pulling experiments with an elastic material of Poisson coefficient $\nu_p = 0.45$, eq. (28) yields a Janssen's constant K_{eff} for the pushing which is about 3% lower than K_{eff} for the pulling. This is qualitatively (though not quantitatively) in agreement with the experimental results.

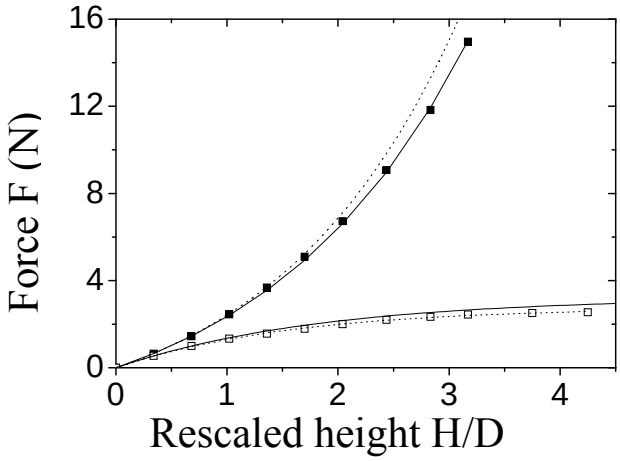


FIG. 27: Resistance force to pushing (filled squares) and to pulling (open squares) in the steady-sliding regime at $V = 16\ \mu\mathrm{m\,s}^{-1}$ as a function of the height H of the packing scaled by the column diameter D, for steel beads in the duralumin column. The lines are the fit with eq. (28) of the resistance force to pushing and its prediction for the pulling situation; the dotted lines are the fit with eq. (28) of the resistance force to pulling and its prediction for the pushing situation.

Therefore isotropic elasticity can be a good framework only if we neglect the existence of bulk restructuring effects inducing differences in the effective Poisson coefficient of the material between the pulling and the pushing. Note that in this case, an isotropic modelling of the granular material is somehow questionable.

H. Towards anisotropy

We have seen in the preceding sections that isotropic elasticity reproduces qualitatively all the features observed in the experiments performed on granular materials. However, some problems remain: a Janssen constant K of order 1.2 was observed experimentally [16] whereas elasticity cannot provide Janssen constants higher than 1.03 with the same experimental parameters (i.e. $\mu_s < 0.3$); moreover, the amplitude of the overshoot predicted by elasticity is 20 times lower than the one observed experimentally.

That is why we study here the predictions of the simplest extension of isotropic elasticity: transversely isotropic elasticity.

The stress-strain relations are now:

$$\epsilon_{xx} = \frac{1}{E_1}\,\sigma_{xx} - \frac{\nu_1}{E_1}\,\sigma_{yy} - \frac{\nu_2}{E_2}\,\sigma_{zz} \tag{29}$$

$$\epsilon_{yy} = -\frac{\nu_1}{E_1}\,\sigma_{xx} + \frac{1}{E_1}\,\sigma_{yy} - \frac{\nu_2}{E_2}\,\sigma_{zz} \tag{30}$$

$$\epsilon_{zz} = -\frac{\nu_2}{E_2}\,\sigma_{xx} - \frac{\nu_2}{E_2}\,\sigma_{yy} + \frac{1}{E_2}\,\sigma_{zz} \tag{31}$$

$$\epsilon_{yz} = \frac{1}{2G}\,\sigma_{yz} \tag{32}$$

$$\epsilon_{xz} = \frac{1}{2G}\,\sigma_{xz} \tag{33}$$

$$\epsilon_{xy} = \frac{(1+\nu_1)}{E_1}\,\sigma_{xy} \tag{34}$$

Following the same calculation steps as in Sec. III A , one can show that, in the limit of high depths z, confinement imposes:

$$\sigma_{rr} = \frac{E_1}{E_2}\frac{\nu_2}{1-\nu_1}\sigma_{zz} \tag{35}$$

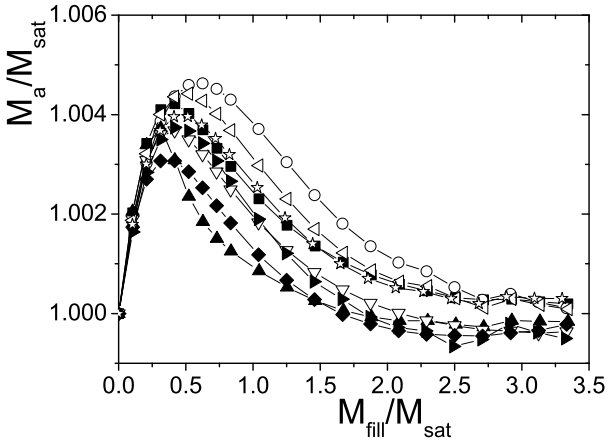


FIG. 28: Apparent mass M_a vs. filling mass M_{fill}, rescaled by the saturation mass M_{sat}, for various transversely isotropic elastic media characterized by the same saturation mass M_{sat}. Squares: $G = 0.345$ MPa, $E_1 = E_2 = 1$ MPa, $\nu_1 = \nu_2 = 0.45$ (isotropic medium). Open circles: $G = 0.1$ MPa, $E_1 = E_2 = 1$ MPa, $\nu_1 = \nu_2 = 0.45$. Triangles: $G = 1$ MPa, $E_1 = E_2 = 1$ MPa, $\nu_1 = \nu_2 = 0.45$. Open down triangles: $G = 0.345$ MPa, $E_1 = 2$ MPa, $E_2 = 1$ MPa, $\nu_1 = \nu_2 = 0.29$. Diamonds: $G = 0.345$ MPa, $E_1 = 2$ MPa, $E_2 = 1$ MPa, $\nu_1 = -0.34$, $\nu_2 = 0.55$. Open left triangles: $G = 0.345$ MPa, $E_1 = 2$ MPa, $E_2 = 1$ MPa, $\nu_1 = 0.756$, $\nu_2 = 0.1$. Right triangles: $G = 0.345$ MPa, $E_1 = 1$ MPa, $E_2 = 2$ MPa, $\nu_1 = 0.633$, $\nu_2 = 0.6$. Open stars: $G = 0.345$ MPa, $E_1 = 1$ MPa, $E_2 = 2$ MPa, $\nu_1 = 0.815$, $\nu_2 = 0.3$. In all these simulations, the friction at the walls is $\mu_s = 0.25$.

i.e. we recover in the anisotropic case a Janssen-like relation between stresses, with a stress redirection constant

$$K_{anis.} = \frac{E_1}{E_2}\frac{\nu_2}{1-\nu_1} \tag{36}$$

The constraints on the elastic parameters are now

$$\nu_1 > -1 \tag{37}$$

$$\nu_1 < \frac{E_1}{E_2} + 1 \tag{38}$$

$$\nu_2^2 < (1-\nu_1)\frac{E_2}{2E_1} \tag{39}$$

We can see the consequences on $K_{anis.}$ through an example. If $\nu_1 = 0$, then the constraint is $\nu_2^2 < \frac{E_2}{2E_1}$ which leads to $K_{anis.} < \sqrt{\frac{E_1}{2E_2}}$. By adjusting the modulus E_1 and E_2, one can give any value to $K_{anis.}$ which is not bounded anymore by a maximum value of 1 (the isotropic case). This means that the experimental values found in [16] for dense packing, i.e. a Janssen constant $K \approx 1.2$, which could not be reached by the isotropic elastic theory, can be understood in the framework of anisotropic elasticity. Note however, that we have now 5 independent parameters instead of 2.

The problem is now that there are several ways to give K a value by adjusting independently (while satisfying the constraints) 4 parameters ν_1, ν_2, E_1, and E_2; another independent parameter is G, which may affect the Janssen profile shape; thus one has to find a physical justification for choosing these values.

We tried to vary independently most parameters while keeping K and μ_s constant in order to see if for a given M_{sat}, there is a way to obtain the giant overshoot we observe experimentally.

Several tries are compared with the isotropic case on Fig. 28. As far as we could see, there is only a rather small influence of anisotropy on the overshoot amplitude: the deviation from the isotropic value is at the most 15% for reasonable values of the modulus. Nevertheless, there are some general tendencies: the higher the shear modulus G, the smaller the overshoot amplitude is; the higher ν_1, the higher the amplitude is, whatever the stiffer direction may be. However, the effect is far from sufficient to reproduce experimental results.

I. A stress induced anisotropy?

In order to account for the height of the experimentally observed overshoot, we propose a toy model based on the idea of stress-induced anisotropy. It is possible that the overweight induces locally a change in the structure. We

would expect an increase of the number of contacts i.e. of the young modulus E_2 in the vertical direction, if the granular material can be modelled as an effective elastic medium. From the relation $K_{anis.} = \frac{E_1}{E_2}\frac{\nu_2}{1-\nu_1}$, we then expect the Janssen coefficient to be lower near the overweight than in the bulk.

Let the Janssen constant be K_1 near the overweight, down to a depth H_1, and $K_2 > K_1$ for any depth $z > H_1$. The saturation mass, which is the overweight mass, was measured with an homogeneous material of Janssen constant K_2 and is thus $M_{sat_2} = \frac{\rho\pi R^3}{2K_2\mu_s}$. Then, it underestimates the saturation mass $M_{sat_1} = \frac{\rho\pi R^3}{2K_1\mu_s}$ of the material layer near the overweight: the measured mass M_a then first increases with the filling mass M_{fill} and would naturally tend to a higher value M_{sat_1}. But for a depth H_1 the material's structure is no more affected by the overweight and is now characterized by a Janssen constant K_2: the mass imposed on the material 2 by the material 1 is then higher than its saturation mass M_{sat_2}, and the measured mass M_a has to decrease with the filling mass M_{fill} in order to reach its saturation value M_{sat_2}.

This simple idea can be easily formalized for an ideal Janssen material. The equilibrium equation on the vertical stress $\sigma_{zz}(z)$ in material i characterized by Janssen constant K_i reads

$$\frac{\partial\sigma_{zz}}{\partial z} + \frac{2K_i\mu_s}{R}\sigma_{zz} = -\rho g \tag{40}$$

In the material 1, for $0 < z < H_1$, we solve this equation for the mass $M(z) = \sigma_{zz}(z)/(\pi R^2 g)$ weighted at depth z, with the boundary condition $M(z{=}0) = M_{sat_2}$ and get

$$M(z) = M_{sat_1}\left(1 - \exp\left(-2K_1\mu_s\frac{z}{R}\right)\right) + M_{sat_2}\exp\left(-2K_1\mu_s\frac{z}{R}\right) \tag{41}$$

In the material 2, for $H_1 < z$ we solve this equation with the boundary condition $M(z = H_1) = M_{sat_1}\big(1 - \exp(-2K_1\mu_s\frac{H_1}{R})\big) + M_{sat_2}\exp(-2K_1\mu_s\frac{H_1}{R})$ and get

$$M(z) = M_{sat_2} + (M_{sat_1} - M_{sat_2})\left(1 - \exp\left(-2K_1\mu_s\frac{H_1}{R}\right)\right)\exp\left(-2K_2\mu_s\frac{(z-H_1)}{R}\right) \tag{42}$$

These equations can be rewritten using M_a/M_{sat_2} and M_{fill}/M_{sat_2} as variables:

$$0 < z < H_1 \rightarrow \frac{M_a}{M_{sat_2}} = \frac{M_{sat_1}}{M_{sat_2}}\left(1 - \exp\left(-\frac{M_{fill}}{M_{sat_2}}\frac{M_{sat_2}}{M_{sat_1}}\right)\right) + \exp\left(-\frac{M_{fill}}{M_{sat_2}}\frac{M_{sat_2}}{M_{sat_1}}\right) \tag{43}$$

$$H_1 < z \rightarrow \frac{M_a}{M_{sat_2}} = 1 + \left(\frac{M_{sat_1}}{M_{sat_2}} - 1\right)\left(1 - \exp\left(-\frac{H_1}{\lambda_2}\frac{M_{sat_2}}{M_{sat_1}}\right)\right)\exp\left(-\left(\frac{M_{fill}}{M_{sat_2}} - \frac{H_1}{\lambda_2}\right)\right) \tag{44}$$

The two independent variables one can adjust are $\frac{M_{sat_1}}{M_{sat_2}}$ (which is the Janssen constant ratio K_2/K_1), and the ratio $H_1/\lambda_2 = M_{fill}(H_1)/M_{sat_2}$ where $\lambda_2 = \rho\pi R/(2K_2\mu_s)$ is the Janssen screening length in the medium 2.

On a $M_a/M_{sat_2} = f(M_{fill}/M_{sat_2})$ plot, the parameter H_1/λ_2 is the X-axis value M_{fill}/M_{sat_2} at which the weighted mass starts to decrease. The slope at the origin is $1 - \frac{M_{sat_2}}{M_{sat_1}}$. Typically (see Fig. 29 and Fig. 30), the experimental slopes are of order 0.5 (it would be 1 for an hydrostatic pressure), i.e. the Janssen coefficient K_1 has to be about 2 times K_2; in the anisotropic elasticity framework, it would mean that the young modulus in the vertical direction is doubled by the overweight. The order of the extension H_1/λ_2 of the induced anisotropy is of order 0.4. The experimental data for dense and loose packing are compared on Fig. 29 and Fig. 30 with the model. It appears to reproduce correctly the data; however, the parameters cannot be determined accurately as they are obtained from the very beginning of the data (the slope at the origin and the X-axis value of the maximum) which cannot be measured with a high precision. Therefore, the parameters presented in these figures are just given as examples.

V. CONCLUSION

In conclusion, we performed an extensive study of the Janssen's column problem. It is a mixture of numerical studies both in 2D and in 3D, in the case of frictional boundaries. The aim was to test thoroughly the classical and celebrated Janssen's analysis in the context of an effective homogeneous elastic material and provide some meaning to the effective Janssen's constant of stress redirection at it can be obtained experimentally. Note that here we do not make any assumption on a plastic threshold in the bulk as it is usually considered to provide bounds on the Janssen's constant (active and passive limits). Also this analysis was performed in the context of an extensive experimental

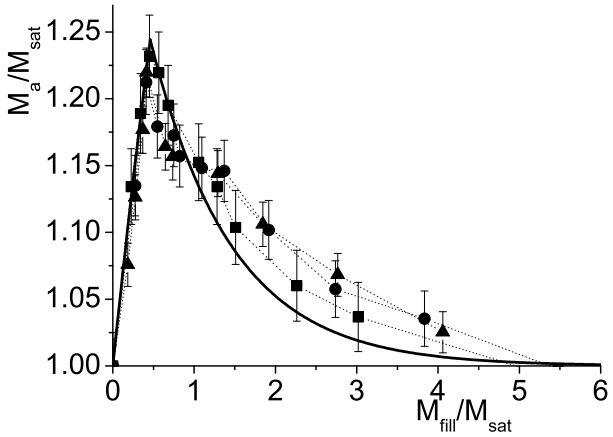


FIG. 29: Apparent mass M_a vs. filling mass M_{fill}, rescaled by the saturation mass M_{sat}, for dense packing in medium-rough columns of 3 diameters (38 mm (squares), 56 mm (circles), 80 mm (triangles)) with an overweight equal to M_{sat}. The data are compared with our inhomogeneous Janssen model with $K_1/K_2 = 2.4$, and $H_1/\lambda_2 = 0.45$.

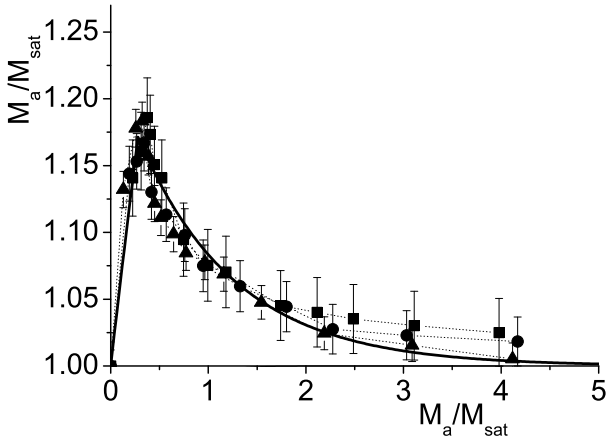


FIG. 30: Apparent mass M_a vs. filling mass M_{fill}, rescaled by the saturation mass M_{sat}, for loose packing in medium-rough columns of 3 diameters (38 mm (squares), 56 mm (circles), 80 mm (triangles)) with an overweight equal to M_{sat}. The data are compared with our inhomogeneous Janssen model with $K_1/K_2 = 2.8$, and $H_1/\lambda_2 = 0.3$.

work where preparation was varied and were special care about friction at the wall was taken to be able to establish a precise comparison with theoretical modelling. Interestingly, we find that the Janssen's approach is fully valid in the limit of low friction coefficients between the grains and the wall (up to a moderate value of 0.5). It means that an exponential saturation curve of the average normal stress at the bottom is an excellent approximation, which defines precisely an effective Janssen's constant solely dependent on the Poisson ratio. We also derive ion the limit of an infinite column a value for an elastic Janssen's constant ($K_{el} = \nu$ in 2D and $K_{el} = \nu/(1-\nu)$ in 3D). For a finite size column, the presence of a bottom diminish the average vertical stress such as to yield an effective Janssen's constant if the bottom normal stress is measured with a value directly related to the elastic constant K_{el}. Therefore, in this context experiment data can be matched with isotropic elasticity if the packing fraction representing the preparation can be associated with an effective Poisson ratio.

Consequently, there is a need to provide a more strained test to the isotropic elastic theory. This was done experimentally by imposing on the top of the column an overweight equal to the saturation stress [16] and here we propose the same test in the same conditions for an elastic material. The numerical simulations show that stresses at the bottom also exhibits an overshoot when the column depth is increased. The relative value of the overshoot is at most 7% . We propose a scaling relation of the overshoot amplitude when the wall fiction is varied. This result contrasts with a Janssen's analysis where a flat profile should be observed. This overshoot effect is related to the deformation of the elastic medium below the overweight which sets a length where the deformation profile is not parabolic any more as in the rest (more like a flat profile as it is imposed by the overweight boundary condition). But at the quantitative level, the overshoot effect found experimentally has an amplitude about 20 to 30 times larger!

This lack of quantitative agreement opens new questions on the modification on the influence of the medium due to the overload. This is the reason why we push further the investigation in the context of anisotropic elasticity. We consider an orthotropic elastic medium with the main stiff direction along the vertical. In this case the effective Janssen's redirection coefficient can be changed according to the stiffness ratio but the overshoot test does not produce an overshoot value significantly larger than the isotropic situation.

Finally, we propose a qualitative model based on an extension of the Janssen's approach where we assume that the overload has changed the medium within a given depth such as to yield a smaller Janssen's constant. This would be consistent with the onset of strain induced anisotropy producing a stiffer medium in the vertical direction. The agreement of this simple model (with two fitting parameters) is satisfactory but more importantly it raises interesting questions and calls for new experimental work. In this frame of mind it would be very interesting to see differences of the stress saturation curve for two media prepared i) with a regular rain like pouring as before and ii) a rain like deposition process but where an overweight is imposed above each deposition step (a deposition step being of a height much smaller than the final height). In this case the stress induced texture changes could provide a rational explanation to the extension of the Janssen's model that fits correctly the overweight experiments.

We thank Profs. R.P. Behringer and J. Socolar for many fruitful discussions.

---

[1] *Physics of Dry Granular Media*, ed. by H.J. Herrmann, J.-P. Hovi and S. Luding, Kluwer Acad. Publisher (1998).
[2] M.Oda, Mechanics of Materials **16**, 35 (1993).
[3] F. Radjai, D.E. Wolf, M. Jean and J.J. Moreau, Phys. Rev. Lett. **80**, 61 (1998).
[4] J. Geng, G. Reydellet, E. Clément and R.P. Behringer, Physica D **182**, 274 (2003).
[5] APF Attman, P. Brunet, J. Geng, G. Reydellet, G. Combe, P. Claudin, R.P. Behringer, E. Clément, *to be published in* J.Cond Mat A (2005); Preprint cond-mat/0411734.
[6] A.J. Liu, S.R. Nagel, Nature 396, 21 (1998).
[7] M.E. Cates, J.P. Wittmer, J.-P. Bouchaud and P. Claudin, Phys. Rev. Lett. **81**, 1841 (1998).
[8] D.M. Wood, *Soil Behaviour and Critical State Soil Mechanics* (Cambridge University, Cambridge, England, 1990).
[9] L. Vanel et al., Phys. Rev. E **60**, R5040 (1999).
[10] J.P. Wittmer, M.E. Cates, P. Claudin, J. Phys. I 7, 39 (1997); J.P. Wittmer et al., Nature **382** , 336 (1996).
[11] G. Reydellet, E. Clément, Phys. Rev. Lett. **86**, 3308 (2001); J. Geng et al., Phys. Rev. Lett. **87**, 035506 (2001); D. Serero et al., Eur. Phys. J. E, **6**, 169 (2001).
[12] H.A. Jannsen, Zeitschr. D. Vereines Deutscher Inginieure **39**, 1045 (1895).
[13] L. Vanel, E. Clément, Eur. Phys. J. B **11**, 525 (1999). L. Vanel et al., Phys. Rev. Lett. **84**, 1439 (2000).
[14] G. Ovarlez, E. Kolb, E. Clément, Phys. Rev. E **64**, 060302(R) (2001).
[15] G. Ovarlez, E. Clément, Phys. Rev. E **68**, 031302 (2003).
[16] G. Ovarlez, C. Fond, E. Clément, Phys. Rev. E **67**, 060302(R) (2003).
[17] E. Kolb, T. Mazozi, E. Clement, and J. Duran, Eur. Phys. J. B, **8**, 483 (1999).
[18] Y. Bertho, F. Giorgiutti-Dauphine, and J.-P. Hulin, Phys. Rev.Lett. **90**, 144301 (2002).
[19] D. Arroyo-Cetto, G. Pulos, R. Zenit and M. A. Jimenez-Zapata, C. R. Wassgren, Phys. Rev. E **68**, 051301 (2003)
[20] J.W. Landry and G.S. Grest, Phys. Rev. E **69**, 031303, (2004).
[21] I. Bratberg, F. Radjai, and A. Hansen, *to be published in* Phys. Rev. E.
[22] D.Senis, C.Allain, Phys. Rev. E **55**, 7797 (1997).
[23] P. Evesque, P.-G. de Gennes, C. R. Acad. Sci. Paris, **326** IIb, 761 (1998).
[24] with CAST3M, http://www-cast3m.cea.fr
[25] C. Goldenberg, I. Goldhirsch, Phys. Rev. Lett. 89, 084302 (2002).